ChemPubSoc Europe

DOI: 10.1002/celc.201500164

CHEMELECTROCHEM Articles

Synthesis of Integrated Layered-Spinel Composite Cathode Materials for High-Voltage Lithium-Ion Batteries up to 5.0 V

Jianqing Zhao, Sarah Ellis, Zhiqiang Xie, and Ying Wang*[a]

Integrated layered-spinel composite materials are synthesized through the facile decomposition of $Li_4Mn_5O_{12}$-based spinel materials at 900 °C. The intergrowth of spinel $Li_{1+z}Mn_{2-z}O_4$ ($0 < z < 0.33$) and Li-rich layered Li_2MnO_3 components is examined by using X-ray diffraction and high-resolution transmission electron microscopy. Such a layered-spinel composite material and its derivatives obtained by doping transition-metal ions are evaluated as high-voltage cathode materials for advanced lithium-ion batteries up to 5.0 V versus Li/Li^+. The Ni-doped composite cathode shows remarkably high-energy and high-power characteristics with high-voltage plateaus at approximately 4.7 V, delivering desirable discharge capacities of 130, 115, and 90 mAh g^{-1} at current densities of 25, 125, and 500 mA g^{-1}, respectively, along with excellent cycling stability. This work provides a facile route for preparing the integrated layered-spinel composite materials as promising high-voltage cathode materials for lithium-ion batteries.

1. Introduction

Lithium-ion batteries have been demonstrated as a feasible power source for hybrid electric vehicles (HEVs) or electric vehicles (EVs). However, large-scale applications of reliable electric transportation still require significant improvement in terms of the energy and power densities of lithium-ion batteries.[1,2] As the traditional graphite anode can almost reach the working potential of lithium metal, finding a high-voltage cathode material is necessary for increasing the operating voltage of lithium-ion batteries and, subsequently, enhancing the energy density.[3,4] The state-of-the-art battery technology is focused on developing novel high-voltage cathode materials with desirable high-rate performance, as the cathode is considered as the limiting factor in lithium-ion batteries, and current lithium-ion batteries show low operating voltages (less than 4.0 V vs. Li/Li^+) as well as poor rate capabilities and unsatisfactory cyclability results.

Among the various cathode materials used, spinel-structured Li–Mn–O oxides offer high voltage plateaus (> 4.6 V vs. Li/Li^+) after substitutions with other transition-metal ions, for example, $Ni^{2+/3+/4+}$, $Co^{3+/4+}$, $Fe^{3+/4+}$, $Cr^{3+/4+}$, and so forth.[3,5,6] In addition, the three-dimensional spinel structure facilitates fast lithium-ion diffusion and provides structural stability during lithiation and delithiation processes, resulting in excellent rate capability and cycling stability. Ni-doped $LiMn_2O_4$, that is, $LiMn_{1.5}Ni_{0.5}O_4$, has been extensively reported in the literature as a high-voltage cathode material.[3–5,7] However, the electrochemical performance of $LiMn_{1.5}Ni_{0.5}O_4$ can easily be affected by impurities,[7a] substituents,[5] crystallinity,[7g] morphology,[2,4,7d,f] and so forth; therefore, rigorous synthetic procedures are required to obtain favorable chemical compositions, structures, and phases. The other great challenge is to manipulate crystal phases of $LiMn_{1.5}Ni_{0.5}O_4$, which has significant effects on the electrochemical performance.[7a] It is difficult to prepare a perfect stoichiometric ordered $P4_332$ phase for $LiMn_{1.5}Ni_{0.5}O_4$, and challenging to prevent an undesirable phase transition from ordered $P4_332$ phase to a nonstoichiometric disordered $Fd\text{-}3m$ phase during electrochemical cycling. Accordingly, strategies involving transition-metal substitutions,[7b,d] extra lithium additions,[7e] surface modifications,[7c] and synthesis controls[7f,g] are still needed to alleviate its unfavorable cycling stability and rate capability. Therefore, it is necessary to explore other facile synthesis methods to develop promising high-voltage cathode materials with remarkable electrochemical performances for batteries used in electric HEVs and EVs.

Two-component integrated composite cathode materials have attracted tremendous research attention for high-capacity lithium-ion batteries,[8] especially the layered–layered composite materials that are rapidly being developed. Typical examples include Li-excess layered transition-metal oxides in a formula of $xLi_2MnO_3{\cdot}(1-x)LiMO_2$ (M = Mn, Ni, Co).[8c,9] For instance, $0.5\ Li_2MnO_3{\cdot}0.5\ LiMn_{1/3}Ni_{1/3}Co_{1/3}O_2$ is composed of two components, that is, layered lithium-inactive Li_2MnO_3 (space group $C2/m$) integrated in the parent phase of layered lithium-active $LiMn_{1/3}Ni_{1/3}Co_{1/3}O_2$ (space group $R\text{-}3m$) with a molar ratio of 1:1.[9a,b] The high capacity of this layered–layered cathode can be achieved through electrochemical activation of inert Li_2MnO_3 during the initial charge above 4.5 V versus Li/Li^+, delivering a specific capacity higher than 250 mAh g^{-1} with a broad operating voltage of up to 4.8 V versus Li/Li^+.[9d] Moreover, the concept of two-component composite cathode materials has been extended to layered-spinel systems.[8b,10,11] The

[a] Dr. J. Zhao, S. Ellis, Z. Xie, Prof. Y. Wang
Department of Mechanical & Industrial Engineering
Louisiana State University
1416 Patrick F. Taylor Hall, Baton Rouge, LA 70803 (USA)
E-mail: ywang@lsu.edu

intergrowth of layered and spinel phases can probably be attributed to the structural compatibility of cubic close-packed oxygen arrays in both layered and spinel structures.[10] Layered-spinel cathode materials, such as 0.7 Li_2MnO_3·0.3 $Li_4Mn_5O_{12}$,[10] and 0.5 Li_2MnO_3·0.5 $Li_4Mn_5O_{12}$,[11] have demonstrated high charge and discharge capacities (> 250 mAh g^{-1}) in a wide voltage range of 2.0–5.0 V versus Li/Li^+. In the layered-spinel system, the layered Li_2MnO_3 component not only contributes to the high capacity, but can also stabilize the spinel component cycled in a broad voltage range after its electrochemical activation during the initial cycle.[11] However, the high capacity is mainly a result of Mn^{3+}/Mn^{4+} redox reactions at 3.0 V. There are few research reports concerning Mn-based layered-spinel composite materials as high-voltage cathodes higher than 4.0 V vs. Li/Li^+) by substituting transition-metal ions.[8b, 10, 12]

There is a compound, spinel $Li_4Mn_5O_{12}$ (marked as S-$Li_4Mn_5O_{12}$), appearing at the composition boundary in the Li–Mn–O phase diagram, which can be used as a promising 3 V cathode material.[13] Furthermore it is well known that S-$Li_4Mn_5O_{12}$ can easily be converted into two components, spinel $Li_{1+z}Mn_{2-z}O_4$ ($0 < z < 0.33$) and Li-rich layered Li_2MnO_3, by annealing at high temperatures above 600 °C.[11, 13a] The electrochemical performance of $Li_{1+z}Mn_{2-z}O_4$ can be significantly improved by integrating it with structurally compatible Li_2MnO_3; hence, in comparison with pure S-Li_4Mn_5O, the composite material, aLi_2MnO_3·$bLi_{1+z}Mn_{2-z}O_4$, attracts more interest, owing to the facile synthesis for layered-spinel integrity after decomposing S-$Li_4Mn_5O_{12}$ at high temperatures. It is also expected that introducing transition-metal ions, such as Ni^{2+} and Co^{3+}, within this two-component compound will result in a high operating voltage together with excellent cyclability and rate capability. Herein, we report a facile route to prepare the integrated layered-spinel composite materials by annealing S-$Li_4Mn_5O_{12}$ spinel and its Ni- and Co-doped compounds at a high temperature of 900 °C. However, it is very difficult to determine the precise chemical composition and phase fraction of layered Li_2MnO_3 and spinel $Li_{1+z}Mn_{2-z}O_4$ components after post-annealing processes. Therefore, we designate the resultant materials as $Li_4Mn_{5-x-y}Ni_xCo_yO_{12}$ (x, $y = 0$ or 0.5) to simplify the case. The electrochemical performance of $Li_4Mn_{5-x-y}Ni_xCo_yO_{12}$ indicates that Co-doping results in significantly enhanced cycling stability of layered-spinel composite cathodes. Meanwhile, Ni-doped compounds show the expected high-voltage characteristics with two voltage plateaus at 4.1 and 4.7 V versus Li/Li^+ along with excellent cycling performance and rate capability, which can be used for large-scale applications in high-energy and high-power lithium-ion batteries.

2. Results and Discussion

The layered-spinel composite materials were prepared by using a sol-gel approach, followed by a post-annealing process. X-ray diffraction (XRD) patterns of the composite materials in Figure 1 reveal the co-existence of layered and spinel phases after sintering the dried gel at a high temperature of 900 °C, during which the pure S-$Li_4Mn_5O_{12}$ spinel is decomposed into spinel $Li_{1+z}Mn_{2-z}O_4$ ($0 < z < 0.33$) and Li-rich layered Li_2MnO_3.[11, 13a] As shown in Figure 1a, the layered Li_2MnO_3 component is indexed from its characteristic peaks with a $C2/m$ symmetry. As the main layered $(001)_L$ peak is mostly overlapped with the spinel $(111)_S$ peak at $2\theta = 18.9°$, the Li_2MnO_3 phase can be identified from other characteristic peaks, such as $(020)_L$ peak at $2\theta = 20.8°$, $(130)_L$ peak at $2\theta = 37.0°$, $(131)_L$ peak at $2\theta = 44.7°$, and $(060)_L$ peak at $2\theta = 65.6°$. On the other hand, the exact composition of the spinel phase is difficult to determine. All characteristic XRD peaks of the spinel phase in Figure 1a are located between standard XRD peaks of spinel $LiMn_2O_4$ (ICDD: 35-0782) and $Li_4Mn_5O_{12}$ (ICDD: 46-0810), indicating a Li/Mn ratio range of 0.5–0.8 in comparison with that of $LiMn_2O_4$ (Li/Mn = 0.5) and $Li_4Mn_5O_{12}$ (Li/Mn = 0.8). As reported in the literature,[13a] the formula of the spinel phase is assigned to $Li_{1+z}Mn_{2-z}O_4$ ($0 < z < 0.33$), and the z value depends on the decomposition conditions of the S-$Li_4Mn_5O_{12}$ spinel

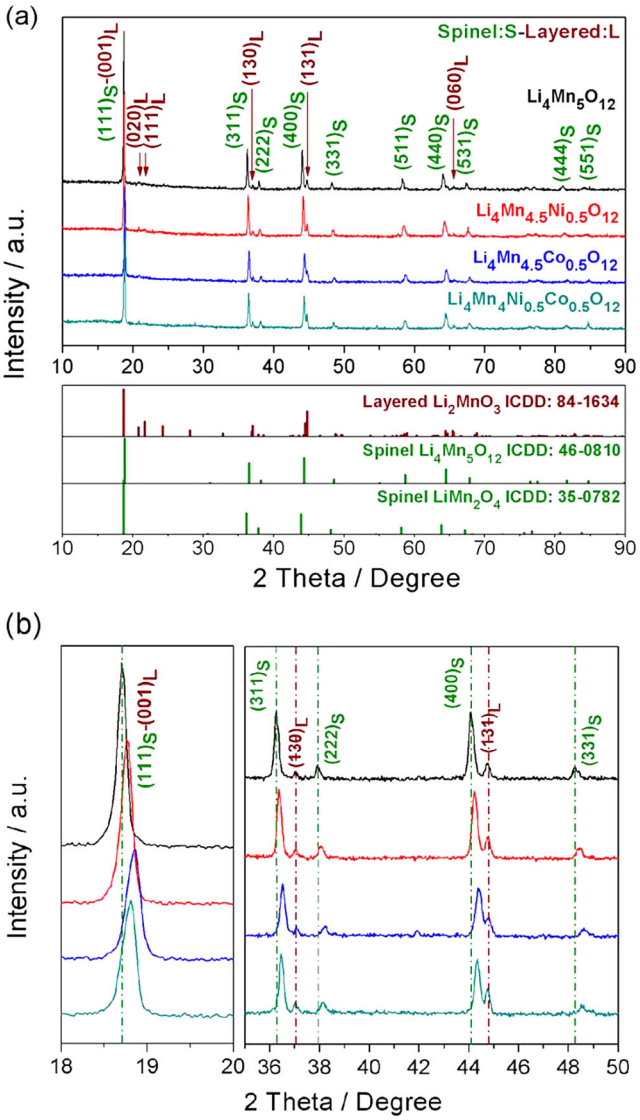

Figure 1. a) XRD patterns and b) selected enlarged portions of $Li_4Mn_5O_{12}$, $Li_4Mn_{4.5}Ni_{0.5}O_{12}$, $Li_4Mn_{4.5}Co_{0.5}O_{12}$, and $Li_4Mn_4Ni_{0.5}Co_{0.5}O_{12}$ in comparison with standard XRD peaks of layered Li_2MnO_3, spinel S-$Li_4Mn_5O_{12}$, and S-$LiMn_2O_4$.

when it is subjected to different heat treatments. Partial replacement of Mn ions with Ni and Co ions show significant effects on the crystal structures of composite materials, but have little influence on co-existence of layered and spinel phases. Figure 1b reveals the selected enlarged portions of XRD patterns in Figure 1a. As shown in the portion at $2\theta = 18–20^\circ$, Ni and Co doping results in XRD peak shifts to higher 2θ reflections of $Li_4Mn_{4.5}Ni_{0.5}O_{12}$, $Li_4Mn_{4.5}Co_{0.5}O_{12}$, and $Li_4Mn_{4.5}Ni_{0.5}Co_{0.5}O_{12}$ in comparison with pristine $Li_4Mn_5O_{12}$, indicating the smaller size of the doped ions compared to Mn ions. The oxidation states of all transition-metal ions will be studied in next section by analyzing their XPS spectra. It is also intriguing to find, in the other selected portion at $2\theta = 36–50^\circ$, that diffraction peak shifts only occur in the spinel phase, involving $(311)_S$, $(222)_S$, $(400)_S$, and $(331)_S$ peaks. In contrast, there is no peak shift of the characteristic $(130)_L$ and $(131)_L$ peaks from the layered Li_2MnO_3 phase before and after doping Ni and/or Co ions in $Li_4Mn_5O_{12}$. Such phenomena suggest the co-existence of a doped spinel component and a preserved layered component in the three resultant compounds of $Li_4Mn_{4.5}Ni_{0.5}O_{12}$, $Li_4Mn_{4.5}Co_{0.5}O_{12}$, and $Li_4Mn_4Ni_{0.5}Co_{0.5}O_{12}$.

Figure 2 presents SEM images of pristine $Li_4Mn_5O_{12}$ particles as well as Ni- and Co-doped compounds. Significant morphological changes are observed, owing to the introduction of Ni and Co ions within the layered-spinel composite materials. As shown in Figure 2a, $Li_4Mn_5O_{12}$ particles exhibit polyhedral shapes and an average particle size of 2 μm. The smooth surface facets reflect high crystallinity of the as-prepared $Li_4Mn_5O_{12}$ particles. Figure 2b reveals that Ni doping drastically reduces the mean particle size of $Li_4Mn_{4.5}Ni_{0.5}O_{12}$ into the submicron scale, whereas Co-doping causes size growth and agglomeration of the resultant $Li_4Mn_{4.5}Co_{0.5}O_{12}$ particles, as shown in Figure 2c. The effects of Co and Ni doping on tailoring the morphology can also be seen in Figure 2d by comparing the morphological features of $Li_4Mn_4Co_{0.5}Ni_{0.5}O_{12}$ particles with $Li_4Mn_{4.5}Ni_{0.5}O_{12}$ (Figure 2b) and $Li_4Mn_{4.5}Co_{0.5}O_{12}$ (Figure 2c) particles. Overall, Ni doping is beneficial as it reduces the particle size of Mn-based layered-spinel composite materials, even after annealing at a high temperature of 900 °C. In contrast, Co doping coarsens the resultant particles and leads to undesirable aggregates.

The XRD results in Figure 1 demonstrate the high crystallinities and co-existence of layered and spinel phases of all samples. The intergrowth of the layered and spinel components in the composite materials is then examined by high-resolution transmission electron microscopy (HRTEM) and corresponding diffraction patterns obtained from live reduced fast Fourier transform (FFT). As shown in Figure 3a, the HRTEM image of $Li_4Mn_5O_{12}$ reveals distinct intergrowth of layered and spinel components with different lattice fringes, in which small layered grains are distributed within a parent and monocrystalline spinel region. The related diffraction pattern in the upper right inset also confirms such two-phase integration from the decomposition of pure spinel S-$Li_4Mn_5O_{12}$, which is consistent with the XRD results (Figure 1). As shown in Figure 3b, the HRTEM image of Ni-doped $Li_4Mn_{4.5}Ni_{0.5}O_{12}$ also shows the intergrowth of layered and spinel components. The corresponding diffraction patterns collected in different regions indicate that regions 1 and 3 have the same layered crystal structures, which are integrated within an entire monocrystalline spinel

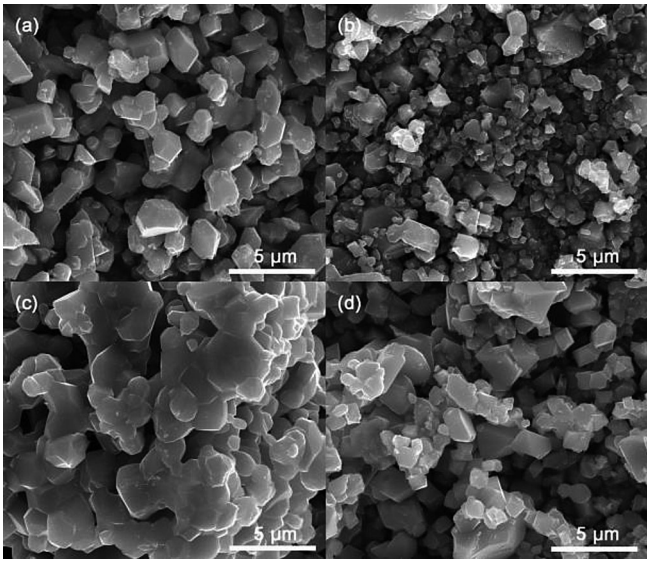

Figure 2. SEM images of a) $Li_4Mn_5O_{12}$, b) $Li_4Mn_{4.5}Ni_{0.5}O_{12}$, c) $Li_4Mn_{4.5}Co_{0.5}O_{12}$ and d) $Li_4Mn_4Ni_{0.5}Co_{0.5}O_{12}$ particles prepared at 900 °C.

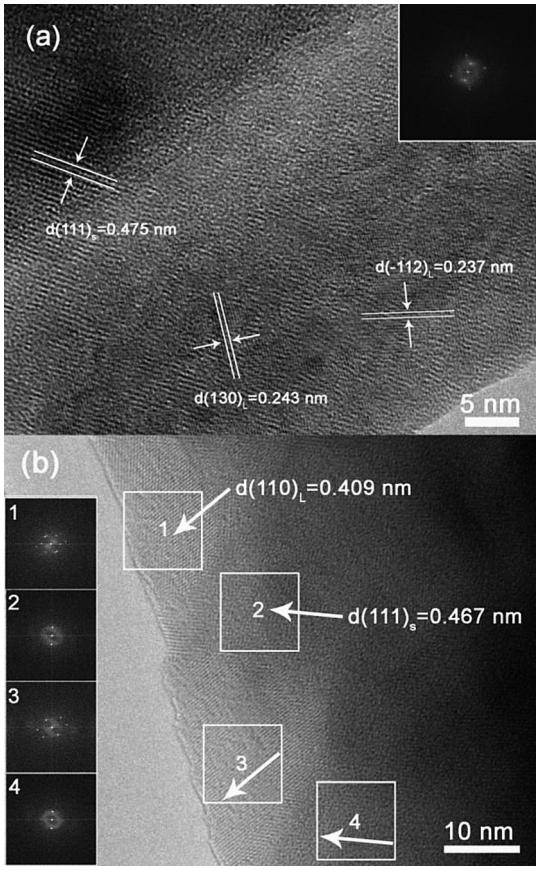

Figure 3. HRTEM images of a) $Li_4Mn_5O_{12}$ and b) $Li_4Mn_{4.5}Ni_{0.5}O_{12}$ showing the intergrowth of layered and spinel components with corresponding diffraction patterns in the insets.

mixture, as indicated in the diffraction patterns of regions 2 and 4. In comparison with pristine $Li_4Mn_5O_{12}$, Ni-doped $Li_4Mn_{4.5}Ni_{0.5}O_{12}$ exhibits a slightly reduced *d*-space distance of $(111)_L$ in the spinel component, which is in agreement with the XRD peak shifts to higher 2θ values (Figure 1b). As a result, it can be concluded that annealing the S-$Li_4Mn_5O_{12}$ spinel at 900 °C is an effective approach to prepare integrated layered-spinel composite materials. There is other ongoing work in our lab to study chemical compositions, that is, to obtain the *z* value of spinel $Li_{1+z}Mn_{2-z}O_4$ ($0<z<0.33$) and the relative molar ratio of layered and spinel components as a result of temperature-dependent annealing processes.

Figure 4 presents the Mn 2p, Ni 2p, and Co 2p XPS spectra of $Li_4Mn_5O_{12}$, $Li_4Mn_{4.5}Ni_{0.5}O_{12}$, $Li_4Mn_{4.5}Co_{0.5}O_{12}$, and $Li_4Mn_4Ni_{0.5}Co_{0.5}O_{12}$ powders to determine the oxidation states of the transition-metal ions in different integrated layered-spinel composite materials. The survey spectra of $Li_4Mn_5O_{12}$ and its doped derivatives in Figure 4a are almost identical to each other, which indicate that the replacement of Mn ions with Ni and/or Co substitutes has little influence on the intergrowth and co-existence of layered and spinel components. However, as shown in Figure 4b–4d, the chemical environments of Mn, Ni, and Co can be effected by each other. Figure 4b reveals the XPS spectra of Mn 2p before and after doping with foreign transition-metal ions. The XPS peaks of Mn $2p_{1/2}$ and Mn $2p_{3/2}$ from pristine $Li_4Mn_5O_{12}$ are located at 654.1 and 642.4 eV, respectively, with a spin–orbital splitting of 11.7 eV. Such peak features indicate that the valence of the Mn ions is mostly tetravalent by indexing to the standard values of MnO_2 (653.9 and 642.2 eV) in the NIST XPS database. The binding-energy difference of 0.2 eV is attributed to the existence of trivalent Mn ions (Mn^{3+}) within the spinel $Li_{1+z}Mn_{2-z}O_4$ ($0<z<0.33$) component. The presence of Mn^{3+} often indicates the existence of disordered spinel structure with a space group of *Fd*-3*m*.[5] As mentioned above, the decomposition products of pure S-$Li_4Mn_5O_{12}$ spinel are spinel $Li_{1+z}Mn_{2-z}O_4$ ($0<z<0.33$) and Li-rich layered Li_2MnO_3 when it is subjected to an annealing temperature above 500 °C.[13a] In our case, the accurate composition of spinel $Li_{1+z}Mn_{2-z}O_4$ and the relative molar ratio of $Li_{1+z}Mn_{2-z}O_4$ to Li_2MnO_3 are very difficult to identify, but the resultant spinel $Li_{1+z}Mn_{2-z}O_4$ has Mn ions with reduced valence, owing to oxygen loss after annealing the S-$Li_4Mn_5O_{12}$ spinel at 900 °C.[10] It is interesting to find that Ni doping leads to a Mn 2p peak shift to a lower binding energy in

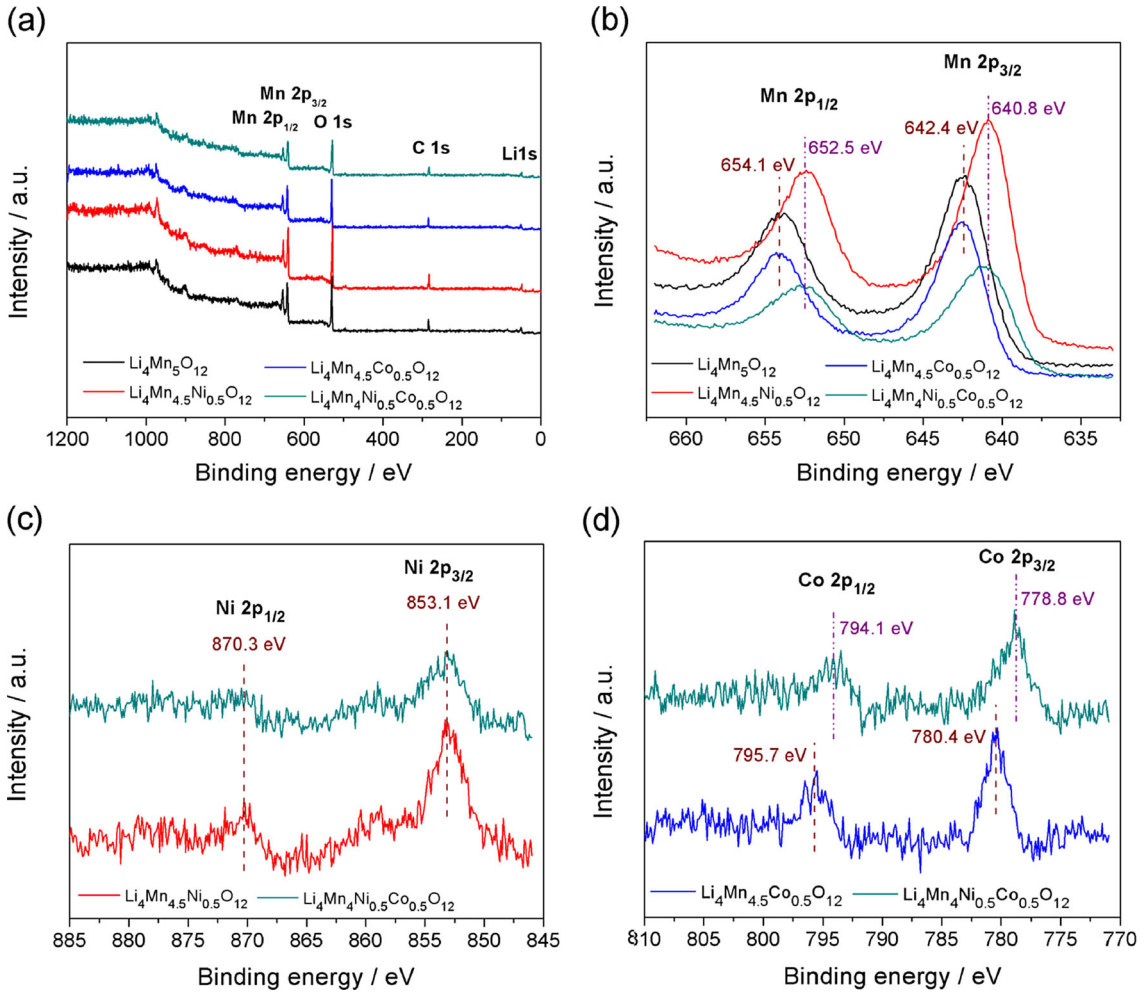

Figure 4. XPS spectra collected from $Li_4Mn_5O_{12}$, $Li_4Mn_{4.5}Ni_{0.5}O_{12}$, $Li_4Mn_{4.5}Co_{0.5}O_{12}$, and $Li_4Mn_4Ni_{0.5}Co_{0.5}O_{12}$ powders: a) survey spectra, b) Mn 2p peaks, c) Ni 2p peaks, and d) Co 2p peaks.

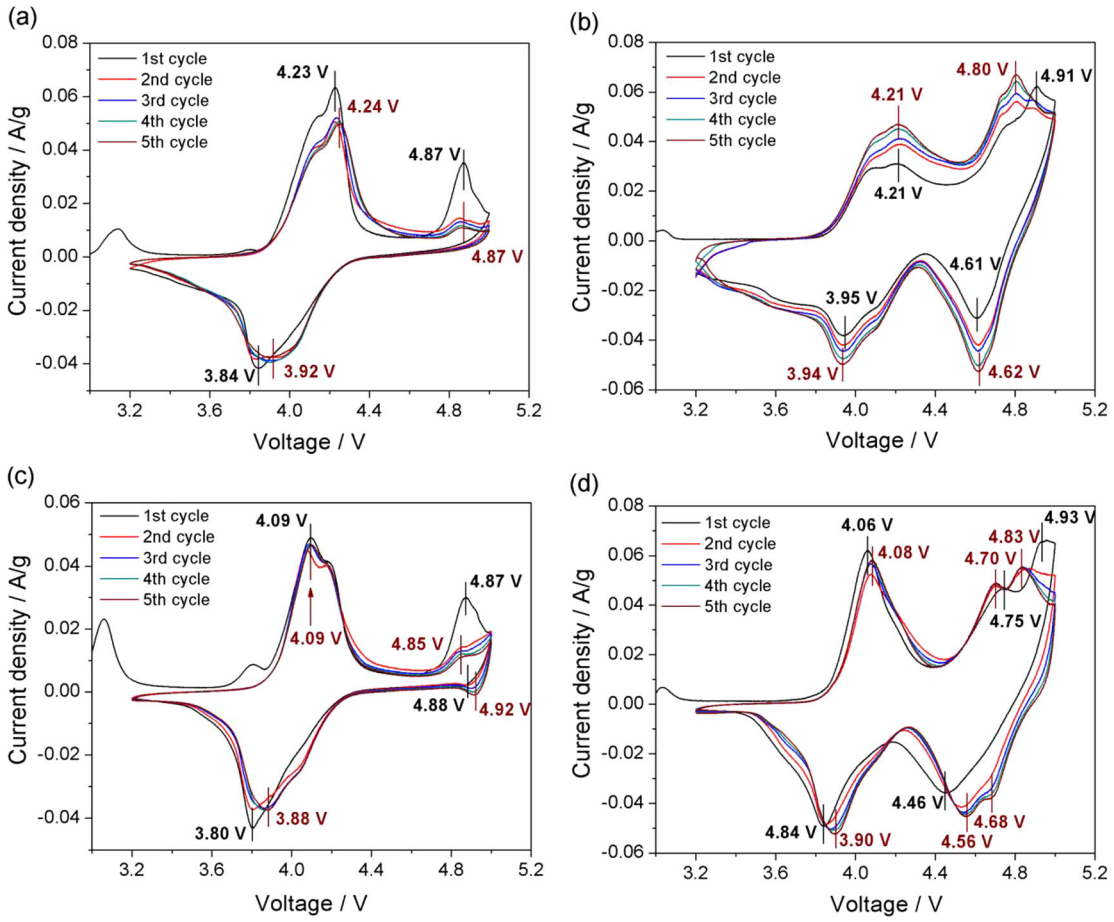

Figure 5. CV curves in the first five cycles of a) $Li_4Mn_5O_{12}$, b) $Li_4Mn_{4.5}Ni_{0.5}O_{12}$, c) $Li_4Mn_{4.5}Co_{0.5}O_{12}$, and d) $Li_4Mn_4Ni_{0.5}Co_{0.5}O_{12}$ at a scan rate of 0.1 mV s^{-1} in a voltage range of 3.2–5.0 V versus Li/Li^+.

$Li_4Mn_{4.5}Ni_{0.5}O_{12}$, whereas Co doping shows no effect on the chemical environment of the Mn ions in $Li_4Mn_{4.5}Co_{0.5}O_{12}$. As shown in Figure 4c, the XPS peaks of Ni 2p in Figure 4c deliver binding energies of 870.3 eV for Ni $2p_{1/2}$ and 853.1 eV for Ni $2p_{3/2}$, indicating the divalence of Ni ions in both $Li_4Mn_{4.5}Ni_{0.5}O_{12}$ and $Li_4Mn_4Ni_{0.5}Co_{0.5}O_{12}$. This result also suggests that further substitutions of Mn ions by Co ions within $Li_4Mn_{4.5}Ni_{0.5}O_{12}$ cannot affect the chemical environment of Ni ions. On the contrary, further replacement of Mn ions with Ni ions within $Li_4Mn_{4.5}Co_{0.5}O_{12}$ has a significant effect on the chemical environment of Co ions. As shown in Figure 4d, the Co XPS spectrum of $Li_4Mn_{4.5}Co_{0.5}O_{12}$ shows binding energies of 795.7 eV for Co $2p_{1/2}$ and 780.4 eV for Co $2p_{3/2}$, indicating that the oxidation state of Co ions is approximately trivalent. However, adding extra Ni ions lowers the binding energies of the Co 2p XPS peaks for $Li_4Mn_{4.5}Ni_{0.5}Co_{0.5}O_{12}$, resulting in a more complicated structure. In summary, the introduction of some transition-metal ions, such as Ni ions in our case, definitely has an impact on the chemical environments of Mn ions in the Mn-based integrated layered-spinel composite material, and thus shows a significant effect on its electrochemical performance.

The electrochemical properties and performance of integrated layered-spinel composite materials are evaluated in a two-electrode system for high-voltage lithium-ion batteries, with a metallic lithium foil as the counter and reference electrodes. Figure 5 shows cyclic voltammetric (CV) curves of $Li_4Mn_5O_{12}$ and its Ni-/Co-doped derivatives in a relatively high voltage range of 3.2–5.0 V versus Li/Li^+. As reported in the literature,[13a] one decomposition product of spinel S-$Li_4Mn_5O_{12}$, that is, spinel $Li_{1+z}Mn_{2-z}O_4$ ($0<z<0.33$), can serve as a 4.0 V cathode, owing to the redox reaction of the $Mn^{3+/}Mn^{4+}$ pair. The initial CV cycle of $Li_4Mn_5O_{12}$ in Figure 5a reveals a main pair, showing an anodic peak at 4.23 V and cathodic peak at 3.84 V, which can be attributed to oxidation and reduction of $Mn^{3+/}Mn^{4+}$ from the spinel $Li_{1+z}Mn_{2-z}O_4$ component, respectively. On the other hand, the layered Li_2MnO_3 component contributes to the anodic peak at 4.87 V in the initial charge process. Such a peak results from the electrochemical activation of Li_2MnO_3 when it is charged above 4.5 V, in which Li_2MnO_3 becomes MnO_2, owing to the extraction of Li^+ in the form of Li_2O.[9a,b,10] In the subsequent CV cycles, CV profiles indicate an outstanding reversibility of the $Mn^{3+/}Mn^{4+}$ pair, but irreversible electrochemical activation of the Li_2MnO_3 component. As a result, the layered-spinel composite cathode material has been demonstrated as a feasible 4.0 V cathode. The XRD patterns in Figure 1 suggest that the replacement of Mn ions with Ni ions only takes place in the spinel $Li_{1+z}Mn_{2-z}O_4$ of $Li_4Mn_{4.5}Ni_{0.5}O_{12}$. As

shown in Figure 5b, in addition to the 4.0 V redox pair, an extra redox couple of approximately 4.7 V is achieved after doping with Ni ions, owing to the introduction of $Ni^{2+}/Ni^{3+}/Ni^{4+}$ redox species in the spinel component.[4] The effects of the initial electrochemical activation and subsequent electrochemical performance of the layered Li_2MnO_3 component are difficult to study, as the voltage range that shows electrochemical behaviors of Li_2MnO_3 is mixed with redox reactions of Ni ions at the voltage range between 4.5 and 5.0 V. It is interesting to see that the current intensities of both 4.0 and 4.7 V redox couples continue to increase from the 2nd cycle to the 5th cycle, which could possibly be ascribed to the stepwise electrochemical activation of Li_2MnO_3 component. Such a phenomenon indicates that Ni doping not only introduces a high operating voltage around 4.7 V, but also can significantly increases the lithium storage capacity of the integrated layered-spinel cathode materials, which offers a facile route to obtain high-energy-density cathode materials for superior lithium-ion batteries.

As shown in Figure 4b, XPS analyses manifest that Co doping reveals little effect on the chemical environment of Mn ions in the intergrowth of layered and spinel phases of $Li_4Mn_{4.5}Co_{0.5}O_{12}$ in comparison with pristine $Li_4Mn_5O_{12}$. Accordingly, CV curves of $Li_4Mn_{4.5}Co_{0.5}O_{12}$ in Figure 5c reveal a very similar profile to that of $Li_4Mn_5O_{12}$ in Figure 5a. In this case, the redox reactions of the Mn^{3+}/Mn^{4+} and Co^{3+}/Co^{4+} couples lead to a broad redox pair around 4.0 V, as the potential of Co^{3+}/Co^{4+} is close to that of Mn^{3+}/Mn^{4+}, and much lower than that of the two-stage $Ni^{2+}/Ni^{3+}/Ni^{4+}$ redox species (ca. 4.7 V). The distinct difference is that there are corresponding cathodic peaks at 4.92 V of $Li_4Mn_{4.5}Co_{0.5}O_{12}$ in subsequent CV cycles after the initial electrochemical activation of Li_2MnO_3. We speculate that the existence of Co ions within the integrated layered-spinel composite cathode can improve the electrochemical reversibility of layered Li_2MnO_3 in the high-voltage region above 4.5 V, in comparison with the irreversible electrochemical behavior of that in pristine $Li_4Mn_5O_{12}$ (Figure 5a). Furthermore, the CV curves of $Li_4Mn_{4.5}Co_{0.5}O_{12}$ after the first two cycles are almost identical, especially at the low voltages of 3.2–4.6 V, indicating excellent cycling stability of such composite cathodes. As reported in the literatures,[14] Co-doping has been demonstrated to enhance electronic conductivity of electrode materials, resulting in reduced electrochemical polarization and improved cyclability, which is consistent with the electrochemical behavior of $Li_4Mn_{4.5}Co_{0.5}O_{12}$ in comparison with $Li_4Mn_5O_{12}$. However, owing to the lager molar mass of Co and the same one-electron transfer of Co^{3+}/Co^{4+} in comparison with Mn^{3+}/Mn^{4+}, substitution of partial Mn ions by Co ions in the electrode materials leads to reduced specific capacities, which is in agreement with the lower current intensities of CV peaks from $Li_4Mn_{4.5}Co_{0.5}O_{12}$ (Figure 5c) compared to that from $Li_4Mn_5O_{12}$ (Figure 5a). Figure 5d reveals the cooperative effects from Ni and Co ions doped in Mn-based layered-spinel composite cathode materials, resulting in significantly enhanced electrochemical reversibility, but showing decreased intensities of the CV peaks of $Li_4Mn_4Co_{0.5}Ni_{0.5}O_{12}$ in the high-voltage region between 4.4 and 5.0 V, which is lower than that of $Li_4Mn_{4.5}Ni_{0.5}O_{12}$. Overall, the CV profiles in Figure 5 demonstrate desirable electrochemical characteristics of the integrated layered-spinel composite cathodes for high-voltage lithium-ion batteries up to 5.0 V.

Figure 6 and Figure 7 present the electrochemical performances of the composite cathode materials in the intergrowth of layered and spinel components, in terms of galvanostatic charge/discharge, cycling performances, and high-rate features. As shown in Figure 6, all voltage plateaus in the charge/discharge curves from four different cathodes are highly consistent with the corresponding CV peaks in Figure 5. As reported in the literature,[10,12b] Li_2MnO_3 and $Li_{1+z}Mn_{2-z}O_4$ ($0<z<0.33$) have the highest theoretical discharge capacity of 225 and 258 mAh g^{-1}, respectively, when they are cycled in a broad voltage range of 2.0–5.0 V versus Li/Li$^+$. However, they can only deliver a discharge capacity below than 100 and 148 mAh g^{-1}, respectively, when cycled in a narrower voltage range of 3.2–5.0 V versus Li/Li$^+$, even after doping with other transition-metal ions, which makes the theoretical capacity of the layered-spinel composite cathode material below 148 mAh g^{-1}. $Li_4Mn_5O_{12}$ reveals predominant discharge voltage plateaus around 4.0 V in Figure 6a after initial electrochemical activation of the layered Li_2MnO_3 component, and can deliver a discharge capacity of 97.2 mAh g^{-1} in the 5th cycle at a current density of 25 mA g^{-1} within a voltage range of 3.2–5.0 V versus Li/Li$^+$. As a result, an estimated energy density of approximately 389 Wh kg^{-1} is obtained for $Li_4Mn_5O_{12}$. In contrast, substitution of Mn ions with Ni ions not only contributes to a higher operating voltage of around 4.7 V, but also considerably increases the energy density of $Li_4Mn_{4.5}Ni_{0.5}O_{12}$. Ni-doped $Li_4Mn_{4.5}Ni_{0.5}O_{12}$ delivers a specific discharge capacity of 129.5 mAh g^{-1} after five cycles, which is composed of approximately 60 mAh g^{-1} at an average voltage of 4.7 V and 70 mAh g^{-1} at an average voltage of 4.0 V. The calculated energy density is approximately 562 Wh kg^{-1}, which is much higher than 389 Wh kg^{-1} of $Li_4Mn_5O_{12}$; hence, the $Li_4Mn_{4.5}Ni_{0.5}O_{12}$ composite material could be considered as a promising high-voltage and high-energy cathode material for superior lithium-ion batteries. Although Co-doping significantly improves the cycling stability of these electrode materials, the relatively low energy densities of approximately 339 Wh kg^{-1} for $Li_4Mn_{4.5}Co_{0.5}O_{12}$ and 446 Wh kg^{-1} for $Li_4Mn_4Ni_{0.5}Co_{0.5}O_{12}$ limit their applications in high-energy lithium-ion batteries. The charge/discharge curves of the 50th and 100th cycle for the four cathodes show no obvious voltage fading and discharge capacity loss, indicating their high structural stability and electrochemical reversibility. Evolution of the charge curves in the high-voltage region above 4.8 V may be attributed to the gradual electrochemical activation of the layered Li_2MnO_3 component, which significantly increases the coulombic efficiency of the cathode materials after 50 cycles.

Accordingly, Figures 7a–7c present the cycling performances and corresponding coulombic efficiencies, rate performances, and electrochemical impedance spectra of the four different cathodes, respectively. It is suggested that the intergrowth of layered and spinel phases benefits the enhanced cycling stability of composite cathode materials, which can be attributed to

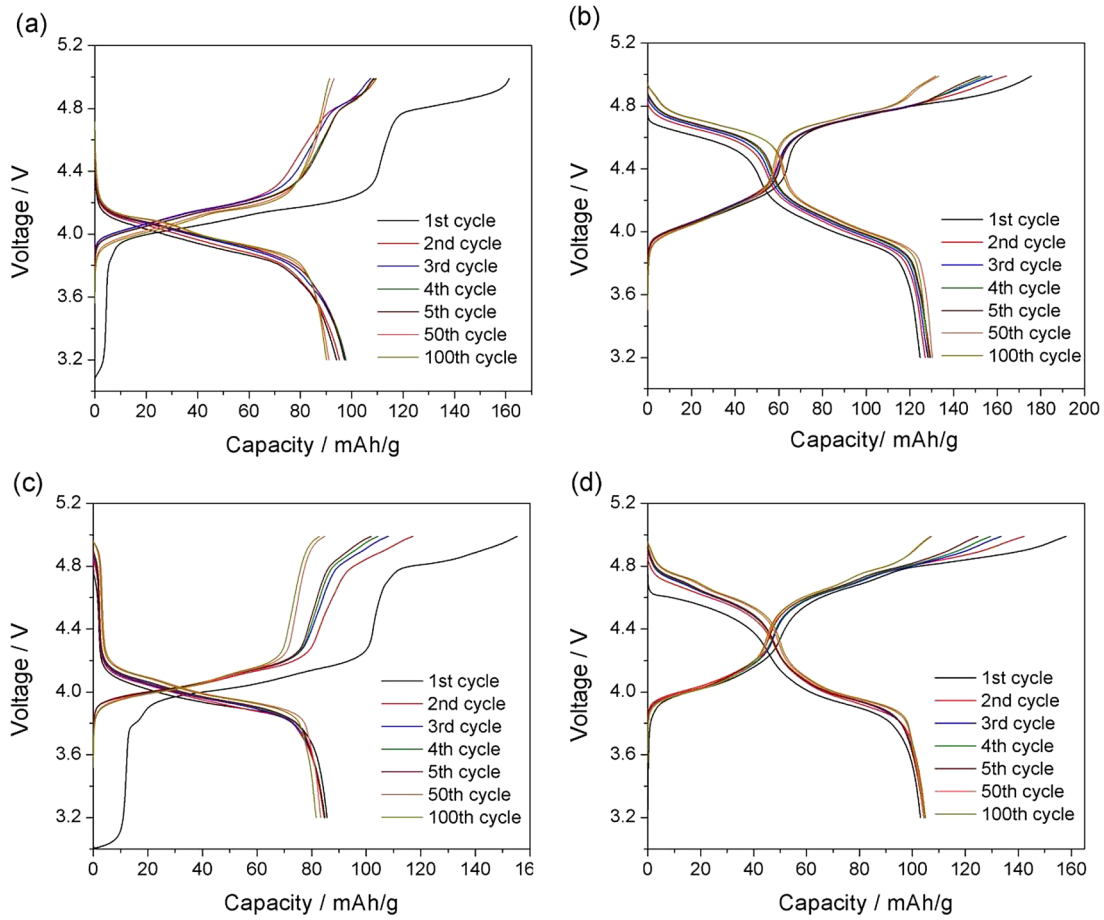

Figure 6. The 1st–5th, 50th, and 100th charge/discharge curves of a) $Li_4Mn_5O_{12}$, b) $Li_4Mn_{4.5}Ni_{0.5}O_{12}$, c) $Li_4Mn_{4.5}Co_{0.5}O_{12}$, and d) $Li_4Mn_4Ni_{0.5}Co_{0.5}O_{12}$ at a specific current of 25 mA g^{-1} in a voltage range of 3.2–5.0 V versus Li/Li^+.

the structural robustness of the cubic spinel component and additional stabilizing effect from the layered Li_2MnO_3 component. As shown in Figure 7a, $Li_4Mn_5O_{12}$ delivers an outstanding discharge capacity retention of 96% after 100 electrochemical cycles at 25 mA g^{-1} in a voltage range of 3.2–5.0 V versus Li/Li^+. After doping with extra transition-metal ions, $Li_4Mn_{4.5}Ni_{0.5}O_{12}$ shows the increased capacity in the first ten cycles up to 132 mAh g^{-1}, probably owing to the capacity contribution from gradual electrochemical activation of Li_2MnO_3, which is approximately 90% of the theoretical capacity (148 mAh g^{-1}) of the layered-spinel composite materials. Such a phenomenon is consistent with the increased current densities of anodic and cathodic peaks during CV cycles in Figure 5b and increased corresponding coulombic efficiencies in Figure 7a. In subsequent electrochemical cycles, this composite cathode exhibits remarkable cycling stability with capacity retention above 98% in the 100th cycle. On the other hand, the effect of Co doping on improving the cyclability, but decreasing the specific capacity, can clearly be seen by comparing the cycling performances of $Li_4Mn_{4.5}Co_{0.5}O_{12}$ and $Li_4Mn_5O_{12}$ as well as $Li_4Mn_4Ni_{0.5}Co_{0.5}O_{12}$ and $Li_4Mn_{4.5}Ni_{0.5}O_{12}$. Figure 7b compares the rate capabilities of different electrodes, revealing electrochemical characteristics that are consistent with the cycling performances in Figure 7a. $Li_4Mn_{4.5}Ni_{0.5}O_{12}$ shows the best rate performance in comparison with the other three cathodes. The desirable discharge capacities of 130, 115, and 90 mAh g^{-1} were achieved at current densities of 25, 125, and 500 mA g^{-1}, respectively. Such excellent rate capability of $Li_4Mn_{4.5}Ni_{0.5}O_{12}$ is probably associated with it having the lowest charge-transfer resistance among all four cathodes, as indicated by the EIS plots in Figure 7c. Furthermore, $Li_4Mn_{4.5}Ni_{0.5}O_{12}$ delivers a high discharge capacity of 100.5 mAh g^{-1} at 1C at 55 °C after 100 electrochemical cycles, along with an outstanding capacity retention of 91.3% in comparison with the highest capacity of 110.4 mAh g^{-1} in the 6th cycle after initial electrochemical activation, as shown in Figure 7d. It is surprising that $Li_4Mn_{4.5}Ni_{0.5}O_{12}$ shows a higher discharge capacity and better cycling stability at elevated temperature (55 °C) compared to room temperature (25 °C) (Figure 7d). Overall, $Li_4Mn_{4.5}Ni_{0.5}O_{12}$ has been demonstrated as a promising alternative cathode material for high-voltage lithium-ion batteries with high energy and power densities, owing to its facile synthesis and remarkable electrochemical performance even at elevated temperatures.

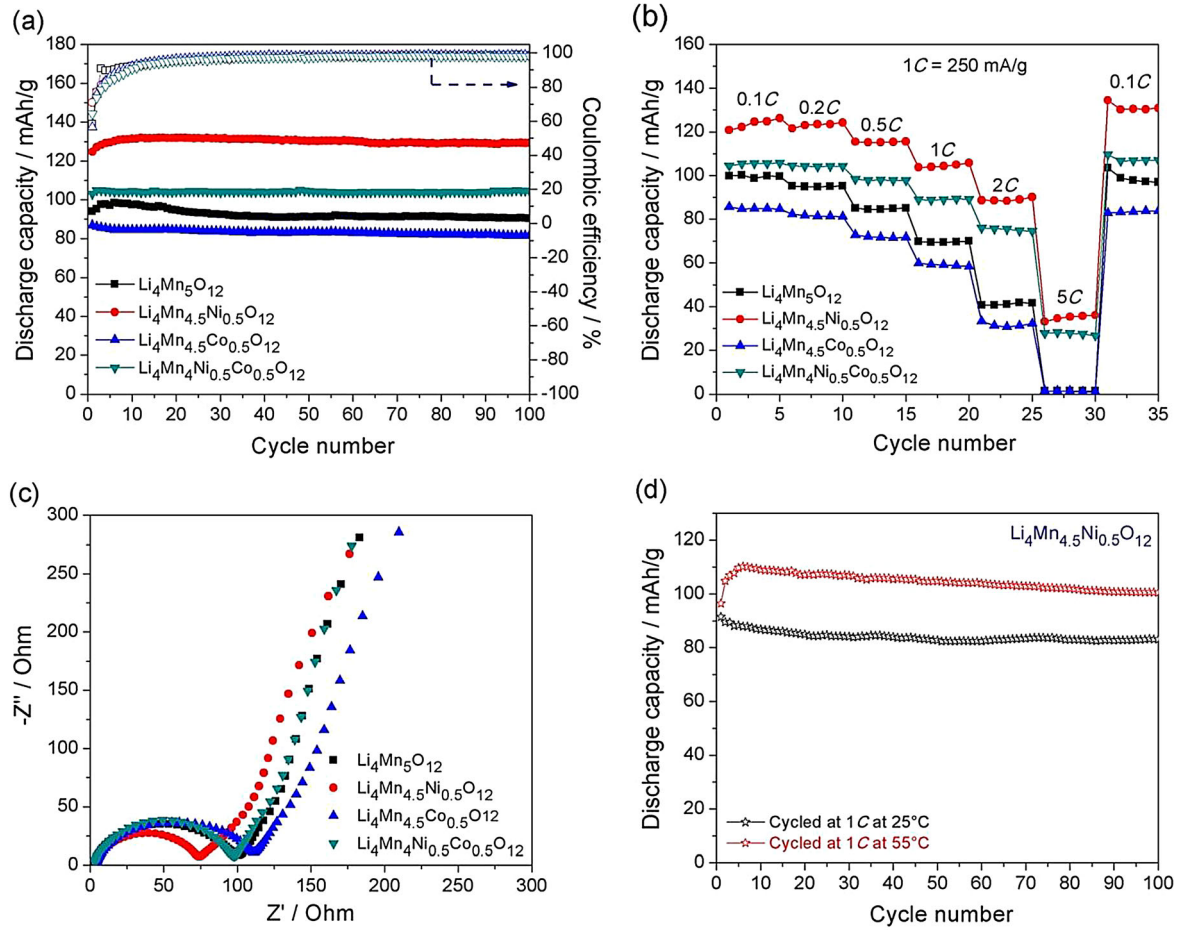

Figure 7. a) Cycling performances at 0.1 C (1 C = 250 mA g^{-1}) with corresponding coulombic efficiencies, b) rate performances at various specific currents (all charges take place at 0.1 C), and c) EIS spectra of $Li_4Mn_5O_{12}$, $Li_4Mn_{4.5}Ni_{0.5}O_{12}$, $Li_4Mn_{4.5}Co_{0.5}O_{12}$, and $Li_4Mn_4Ni_{0.5}Co_{0.5}O_{12}$ in a voltage range of 3.2–5.0 V versus Li/Li^+. d) Cycling performance of $Li_4Mn_{4.5}Ni_{0.5}O_{12}$ at 55 °C at 1 C in a voltage range of 3.2–5.0 V versus Li/Li^+ in comparison with that at 25 °C.

3. Conclusions

The integrated spinel $Li_{1+z}Mn_{2-z}O_4$ ($0 < z < 0.33$) and layered Li_2MnO_3 composite material is prepared by decomposing the pure S-$Li_4Mn_5O_{12}$ spinel material at a high annealing temperature. The intergrowth of layered and spinel components is demonstrated by using XRD and HRTEM characterization. The XRD results further indicate that doping the layered-spinel composite material with transition-metal ions (Ni and Co ions) results in a doped spinel component and preserved layered Li_2MnO_3. Partial substitution of Mn ions by Ni or Co ions shows distinct effects on the particle size, crystal structure, and chemical environment of Mn ions in the resultant doped compounds. The electrochemical performances of the integrated layered-spinel composite material and its doped compounds are evaluated as cathode materials for high-voltage lithium-ion batteries up to 5.0 V. The pristine Mn-based layered-spinel composite cathode showed voltage plateaus at approximately 4.0 V. Introduction of Co ions led to enhanced cycling stability, but decreased specific capacity of the composite cathodes. In contrast, Ni doping not only resulted in a significantly higher 4.7 V operating voltage plateau, but also led to excellent cycling stability and rate capability of the final cathode, delivering a high specific discharge capacity of approximately 130 mAh g^{-1} and corresponding energy density above 560 Wh kg^{-1}. Therefore, the Ni-doped layered-spinel composite material is demonstrated as a high-voltage cathode material with desirable energy and power densities.

Experimental Section

Synthesis of Layered-Spinel Integrated Composite Materials

Layered-spinel integrated composite materials with the formula $Li_4Mn_{5-x-y}Ni_xCo_yO_{12}$ (x, $y = 0$ or 0.5) were synthesized by using a facile sol-gel method. We first prepared two precursor solutions: 20 mmol transition metal (II) acetate tetrahydrates [a molar ratio of $Mn^{2+}/Ni^{2+}/Co^{2+} = (5-x-y)/x/y$] in 50 mL distilled water, and 16 mmol lithium hydroxide in 15 mL distilled water. The transition-metal precursor solution was added dropwise into the lithium precursor solution under continuous stirring. The mixed solution was then heated at 80 °C until the solvent was completely evaporated. Afterwards, the mixture was dried in air at 120 °C for 12 h. Heat treatment of the dried mixture was carried out in air at 500 °C for

5 h, followed by sintering at 900 °C for 3 h. The as-prepared particles were collected after cooling to room temperature.

Characterizations

The crystallographic structures of the layered-spinel composite materials were examined by using XRD with a Rigaku MiniFlex X-ray diffractometer with CuK_α radiation at a scan rate of $2^\circ\,min^{-1}$. The morphology and particle size of different particles were observed by using FEI Quanta 3D FEG field-emission scanning electron microscopy. TEM images were captured on a JEOL JEM-2010 microscope at an acceleration voltage of 200 kV to investigate the structures of $Li_4Mn_{5-x-y}Ni_xCo_yO_{12}$ particles. Chemical valences of Mn, Ni, and Co within the compounds were analyzed by using an X-ray photoelectron spectroscope with an AXIS 165 spectrometer and a twin-anode AlK_α (1486.6 eV) X-ray source. All XPS spectra were calibrated according to the binding energy of the C 1s peak at 284.8 eV.

Electrochemical Measurements

The working electrodes were composed of 80 wt% $Li_4Mn_{5-x-y}Ni_xCo_yO_{12}$ particles, 10 wt% acetylene black (conductive carbon, Alfa Aesar, 99.5%), and 10 wt% poly-vinylidenefluoride (PVDF, Alfa Aesar) as the binder. The cathodes were assembled into two-electrode CR2032-type coin cells for electrochemical measurements, with a metallic lithium foil as the anode, and Celgard-2320 membrane as the separator; the electrolyte was 1 M $LiPF_6$ dissolved in ethylene carbonate (EC), dimethyl carbonate (DMC), and diethyl carbonate (DEC) at a volumetric ratio of 1:1:1. Galvanostatic charge and discharge processes were performed at different current densities in a voltage range of 3.2–5.0 V by using an eight-channel battery analyzer (MTI Corporation). Electrochemical storage capacities of the working electrodes were calculated based on the mass of active cathode materials. CV curves of the different cathodes were recorded at a scan rate of 0.1 $mV\,s^{-1}$ between 3.2 and 5.0 V versus Li/Li^+ and EIS spectra of the cathodes were obtained in a frequency range of 10^{-2}–10^5 Hz with an amplitude of 5 mV, using an electrochemical analyzer (CHI 605C).

Acknowledgements

This work is supported by a LaSPACE-REA grant. The authors also acknowledge LSU IAM Shared Instrumentation Facility (SIF) at Louisiana State University for characterizations.

Keywords: cationic substitution · conducting materials · high-voltage cathode materials · lithium-ion batteries · spinel phases

[1] J. Xu, S. Dou, H. Liu, L. Dai, *Nano Energy* **2013**, *2*, 439–442.
[2] Y. Qian, Y. Deng, Z. Shi, Y. Zhou, Q. Zhuang, G. Chen, *Electrochem. Commun.* **2013**, *27*, 92–95.
[3] A. Manthiram, K. Chemelewski, E. S. Lee, *Energy Environ. Sci.* **2014**, *7*, 1339.
[4] X. Fang, M. Ge, J. Rong, C. Zhou, *ACS Nano* **2014**, *8*, 4876–4882.
[5] Y. P. Zeng, X. L. Wu, P. Mei, L.-N. Cong, C. Yao, R.-S. Wang, H.-M. Xie, L. Q. Sun, *Electrochim. Acta* **2014**, *138*, 493–500.
[6] A. R. West, H. Kawai, H. Kageyama, M. Tabuchi, M. Nagata, H. Tukamoto, *J. Mater. Chem.* **2001**, *11*, 1662–1670.
[7] a) J. H. Kim, A. Huq, M. Chi, N. P. W. Pieczonka, E. Lee, C. A. Bridges, M. M. Tessema, A. Manthiram, K. A. Persson, B. R. Powell, *Chem. Mater.* **2014**, *26*, 4377–4386; b) N. Kiziltas-Yavuz, A. Bhaskar, D. Dixon, M. Yavuz, K. Nikolowski, L. Lu, R. A. Eichel, H. Ehrenberg, *J. Power Sources* **2014**, *267*, 533–541; c) H. Konishi, K. Suzuki, S. Taminato, K. Kim, Y. Zheng, S. Kim, J. Lim, M. Hirayama, J. Y. Son, Y. Cui, R. Kanno, *J. Power Sources* **2014**, *269*, 293–298; d) H. Wang, T. A. Tan, P. Yang, M. O. Lai, L. Lu, *J. Phys. Chem. C* **2011**, *115*, 6102–6110; e) Y. Qian, Y. Deng, L. Wan, H. Xu, X. Qin, G. Chen, *J. Phys. Chem. C* **2014**, *118*, 15581–15589; f) J. Yang, X. Zhang, Z. Zhu, F. Cheng, J. Chen, *J. Electroanal. Chem.* **2013**, *688*, 113–117; g) W. W. Wu, H. F. Xiang, G. B. Zhong, W. Su, W. Tang, Y. Zhang, Y. Yu, C. H. Chen, *Electrochim. Acta* **2014**, *119*, 206–213.
[8] a) M. M. Thackeray, C. S. Johnson, J. T. Vaughey, N. Li, S. A. Hackney, *J. Mater. Chem.* **2005**, *15*, 2257–2267; b) E. S. Lee, A. Huq, H. Y. Chang, A. Manthiram, *Chem. Mater.* **2012**, *24*, 600–612; c) A. Boulineau, L. Simonin, J. F. Colin, E. Canévet, L. Daniel, S. Patoux, *Chem. Mater.* **2012**, *24*, 3558–3566; d) D. Kim, G. Sandi, J. R. Croy, K. G. Gallagher, S. H. Kang, E. Lee, M. D. Slater, C. S. Johnson, M. M. Thackeray, *J. Electrochem. Soc.* **2012**, *160*, A31–A38.
[9] a) N. Yabuuchi, K. Yoshii, S. T. Myung, I. Nakai, S. Komaba, *J. Am. Chem. Soc.* **2011**, *133*, 4404–4419; b) F. Amalraj, M. Talianker, B. Markovsky, D. Sharon, L. Burlaka, G. Shafir, E. Zinigrad, O. Haik, D. Aurbach, J. Lampert, M. Schulz-Dobrick, A. Garsuch, *J. Electrochem. Soc.* **2012**, *160*, A324–A337; c) M. N. Ates, Q. Jia, A. Shah, A. Busnaina, S. Mukerjee, K. M. Abraham, *J. Electrochem. Soc.* **2013**, *161*, A290–A301; d) D. Wang, I. Belharouak, X. Zhang, Y. Ren, G. Meng, C. Wang, *J. Electrochem. Soc.* **2014**, *161*, A1–A5.
[10] C. S. Johnson, N. Li, J. T. Vaughey, S. A. Hackney, M. M. Thackeray, *Electrochem. Commun.* **2005**, *7*, 528–536.
[11] J. Cao, J. Xie, G. Cao, T. Zhu, X. Zhao, S. Zhang, *Electrochim. Acta* **2013**, *111*, 447–454.
[12] a) P. K. Nayak, J. Grinblat, M. D. Levi, O. Haik, E. Levi, M. Talianker, B. Markovsky, Y. K. Sun, D. Aurbach, *Chem. Mater.* **2015**, *27*, 2600–2611; b) J. Cabana, C. S. Johnson, X. Q. Yang, K. Y. Chung, W. S. Yoon, S. H. Kang, M. M. Thackeray, C. P. Grey, *J. Mater. Res.* **2010**, *25*, 1601–1616; c) J. Cabana, S. H. Kang, C. S. Johnson, M. M. Thackeray, C. P. Grey, *J. Electrochem. Soc.* **2009**, *156*, A730–A736.
[13] a) Y. Xia, M. Yoshio, *J. Electrochem. Soc.* **1997**, *144*, 4186–4194; b) Y. Fu, H. Jiang, Y. Hu, L. Zhang, C. Li, *J. Power Sources* **2014**, *261*, 306–310; c) Y. Tian, D. Chen, X. Jiao, Y. Duan, *Chem. Commun.* **2007**, 2072–2074; d) Y. P. Jiang, J. Xie, G. S. Cao, X. B. Zhao, *Electrochim. Acta* **2010**, *56*, 412–417.
[14] A. D. Robertson, A. R. Armstrong, P. G. Bruce, *J. Power Sources* **2001**, *97–98*, 332–335.

Received: April 18, 2015
Revised: June 2, 2015
Published online on ■■ ■■, 2015

ARTICLES

*J. Zhao, S. Ellis, Z. Xie, Y. Wang**

■■ – ■■

Synthesis of Integrated Layered-Spinel Composite Cathode Materials for High-Voltage Lithium-Ion Batteries up to 5.0 V

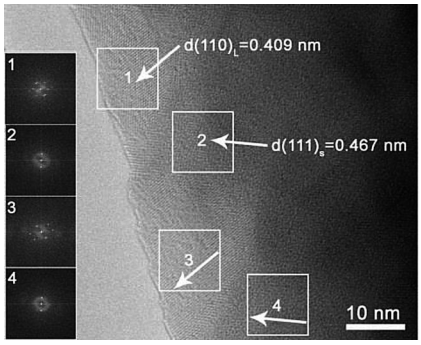

LIB up to expectations: Integrated layered-spinel composite materials are prepared through the decomposition of $Li_4Mn_5O_{12}$-based spinel materials at high annealing temperature. After doping with additional transition metal ions, such layered-spinel compounds can serve as high-voltage cathode materials for advanced lithium-ion batteries up to 5.0 V versus Li/Li^+. The Ni-doped composite cathode shows remarkably high-energy and high-power characteristics, along with excellent cycling stability.